

Article

Calcium Delivery by Electroporation Induces In Vitro Cell Death through Mitochondrial Dysfunction without DNA Damages

Laure Gibot ^{1,†} , Audrey Montigny ¹, Houda Baaziz ¹, Isabelle Fourquaux ², Marc Audebert ^{3,*} 
and Marie-Pierre Rols ^{1,*} 

¹ Institut de Pharmacologie et de Biologie Structurale, Université de Toulouse, CNRS, UPS, 31077 Toulouse, France; gibot@ipbs.fr (L.G.); montigny@ipbs.fr (A.M.); baaziz@ipbs.fr (H.B.)

² Centre de Microscopie Électronique Appliquée à la Biologie, CMEAB, 133 route de Narbonne, 31062 Toulouse CEDEX, France; isabelle.fourquaux@univ-tlse3.fr

³ Toxalim, Université de Toulouse, INRAE-UMR1331, ENVT, INP-Purpan, UPS, 31027 Toulouse, France

* Correspondence: marc.audebert@inrae.fr (M.A.); rols@ipbs.fr (M.-P.R.)

† Current address: Laboratoire des IMRCP, Université de Toulouse, CNRS UMR 5623, Université Toulouse III-Paul Sabatier, 31062 Toulouse, France; gibot@chimie.ups-tlse.fr (L.G.).

Received: 21 January 2020; Accepted: 6 February 2020; Published: 12 February 2020



Abstract: Adolescent cancer survivors present increased risks of developing secondary malignancies due to cancer therapy. Electrochemotherapy is a promising anti-cancer approach that potentiates the cytotoxic effect of drugs by application of external electric field pulses. Clinicians proposed to associate electroporation and calcium. The current study aims to unravel the toxic mechanisms of calcium electroporation, in particular if calcium presents a genotoxic profile and if its cytotoxicity comes from the ion itself or from osmotic stress. Human dermal fibroblasts and colorectal HCT-116 cell line were treated by electrochemotherapy using bleomycin, cisplatin, calcium, or magnesium. Genotoxicity, cytotoxicity, mitochondrial membrane potential, ATP content, and caspases activities were assessed in cells grown on monolayers and tumor growth was assayed in tumor spheroids. Results in monolayers show that unlike cisplatin and bleomycin, calcium electroporation induces cell death without genotoxicity induction. Its cytotoxicity correlates with a dramatic fall in mitochondrial membrane potential and ATP depletion. Opposite of magnesium, over seven days of calcium electroporation led to spheroid tumor growth regression. As non-genotoxic, calcium has a better safety profile than conventional anticancer drugs. Calcium is already authorized by different health authorities worldwide. Therefore, calcium electroporation should be a cancer treatment of choice due to the reduced potential of secondary malignancies.

Keywords: calcium electroporation; electrochemotherapy; spheroids; magnesium; genotoxicity; mitochondria

1. Introduction

An alternative approach to classical chemotherapy, electrochemotherapy (ECT), has developed in recent decades and is currently used in more than 150 centers and clinics throughout Europe [1]. Electrochemotherapy treatment was standardized in the framework of the European Standard Operating Procedure on Electrochemotherapy (ESOPE) multicenter trial, first released in 2006 and recently updated [2]. It consists of associating cytotoxic drug injection with the application of calibrated electric field pulses delivered locally at the tumor site. Indeed, in the 1970s, it was demonstrated that the application of calibrated external electric field pulses can transiently permeabilize the vesicular cell membrane [3]. Further developments of this approach showed that transient permeabilization of

the plasma membrane allows non-permeant or low permeant cytotoxic drugs to enter the cytoplasm in large quantities and thus potentiate its activity. The proof of concept was led with bleomycin, a non-permeant molecule with a very high molecular weight and intrinsic cytotoxicity which was dramatically enhanced by 700-fold after electroporation, compared to the drug alone [4]. On the contrary, only a 1.1–1.3-fold increase of cytotoxicity was observed with lipophilic drugs able to rapidly diffuse through the plasma membrane, such as vinblastine [5]. This enhanced cytoplasmic penetration, spatially and temporarily localized in the tissue between the electrodes diminishes the quantity of injected antitumor drugs, thus limiting short-term and long-term side effects. Nowadays, electrochemotherapy is associated with the application of external electric field pulses and injection of hydrophilic drugs such as bleomycin and cisplatin. A study comparing the efficiency of electrochemotherapy of cisplatin with intratumoral administration of cisplatin alone on cutaneous tumor lesions in breast cancer indicated that ECT displayed a better complete objective response to treatment than cisplatin alone (100% and 83%, respectively), with 33% complete response for ECT and 0% for cisplatin alone [6]. Interestingly, according to a recent meta-analysis of all available clinical data on electrochemotherapy, the objective treatment response of evaluated studies was 83.91% (95% CI: 79.15–88.17%) for bleomycin and 80.82% (95% CI: 66.00–92.36%) for cisplatin [7] with a good preservation of healthy tissues. Long-term effects of electrochemotherapy are still to be determined, as the potential occurrence of secondary malignancies has never been reported until now, after more than a decade of use.

During the last years, calcium electroporation was proposed as a potential novel anticancer treatment, where high concentrations of calcium (CaCl_2) are introduced in cell cytoplasm thanks to electroporation, inducing cell necrosis. This innovative approach already demonstrated its efficiency in vitro on two-dimensional (2D) cell monolayer, in 3D spheroid tumor model, in vivo, and in human clinical studies [8–12]. This treatment modality is fairly easy to implement. Calcium is injected locally into the tumors and electric pulses are administered immediately thereafter. Recently, a randomized double-blinded phase II study compared calcium electroporation with bleomycin electrochemotherapy against cutaneous metastasis [11]. There was no statistically significant difference between the two treatments. Remarkably, calcium electroporation presented fewer secondary effects than electrochemotherapy (itching, exudation, hyperpigmentation). Calcium electroporation was also shown as a safe treatment on mucosal head and neck cancers with no signs of hypercalcemia, cardiac arrhythmias, or severe adverse events [12]. Perspectives for calcium electroporation are therefore highly promising.

Based on that, our study proposes to answer two specific questions in order to better understand cellular toxic mechanisms induced by calcium electroporation and keep promoting its use as a safe, efficient, and innovative antitumor treatment. First, does calcium electroporation treatment, in addition to being cytotoxic, present a genotoxic profile like other classical antitumor drugs such as cisplatin or bleomycin? Bleomycin as well as cisplatin are used to set up the genotoxic assay and validate the proven effectiveness of electroporation with these two drugs. Second, is the cytotoxic effect of calcium electroporation specifically due to calcium ion or to the osmolarity of the solution? Magnesium (MgCl_2) solutions at the same osmolarity as calcium (CaCl_2) solutions were used to treat the cells and find responses.

To answer these questions, we used human normal primary dermal fibroblasts and human colorectal cancer cell line HCT-116. The first part of the study was led on cell cultures grown in 2D monolayers. The other part was led on a 3D tumor model named spheroid, particularly suitable for in vitro study of electroporation [13–15] and closer to in vivo reality than monolayers [16].

2. Results

2.1. Determination of Optimal Electrical Parameters to Induce Reversible Cell Electroporabilization

Typical electrical parameters used in electrochemotherapy are eight pulses lasting 100 μs , applied at 1 Hz frequency [17]. The electric field intensity to apply to efficiently induce reversible plasma

membrane permeabilization without affecting cell viability depends on the cell type and cell organization (in 2D or in 3D models) and therefore has to be determined before the experiment. For normal dermal fibroblasts and tumor HCT-116 cells grown in monolayers, a 500 V/cm intensity appeared to be the optimal value (Figure 1).

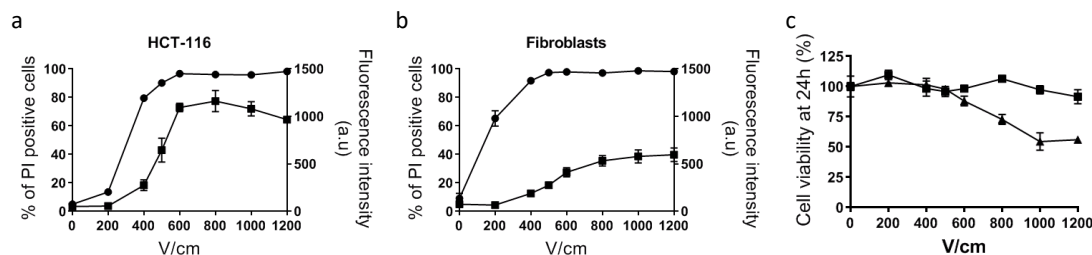


Figure 1. Determination of optimal voltage leading to reversible cell electropermeabilization. Cell electropermeabilization assessed by flow cytometry in HCT-116 tumor cells (a) and normal dermal fibroblasts (b), $n = 3$. Circles indicate the % of cells labeled with propidium iodide used as a marker of plasma membrane permeabilization. Squares indicate the mean fluorescence intensity (arbitrary units) of positive cells to propidium iodide. (c) Cell viability quantified with PrestoBlue assay based on cell metabolism, 24 h after application of electric pulses. Squares: fibroblasts; triangles: HCT-116; $n = 3$.

In this condition, more than 90% of cells were efficiently electropermeabilized, as determined by propidium iodide uptake, while their viability was unaffected. In 3D colorectal tumor spheroids, cells display a distinct shape and size than in monolayers and therefore require different electric field intensity. We took advantage of our previous study and choose 1000 V/cm as the optimum intensity allowing efficient electropermeabilization while ensuring cell viability [9].

2.2. Electrochemotherapy Potentiates Genotoxic and Cytotoxic Effects of Cisplatin and Bleomycin, both in Normal and Tumor Cells

Whether for tumor HCT-116 cells or for normal dermal fibroblasts, cisplatin and bleomycin were genotoxic as revealed by induction of the phosphorylation of histone H2AX, a biomarker of global DNA damage [18]. As shown in Figure 2, compared to the control, a significant increase in genotoxicity appeared above 10 μM for cisplatin alone and 50 nM for bleomycin alone in a concentration-dependent manner of the antitumor drugs cisplatin (1, 10, 50, 100 μM) and bleomycin (5, 50, 500, 1000 nM). When associated with electroporation, the genotoxicity of cisplatin tended to increase but statistical significance was not observed. In this experimental condition, a significant decrease in the viability of cancer cells was observed, while this effect was not statistically significant for normal dermal fibroblasts. Concerning bleomycin, it is obvious that the association with electroporation hugely potentiated both its genotoxic and cytotoxic effects. Indeed, even the lowest concentration of bleomycin (i.e., 5 nM) induced genotoxicity in HCT-116 cells (1.6-fold induction of γH2AX compared to control condition), but when associated with electroporation, it raised to 7.5-fold. Similarly, for 50 nM of bleomycin in normal fibroblasts, fold induction of γH2AX switched from 2 when incubated alone to 14 when associated with electroporation. Increasing genotoxic effect was also correlated with a higher cytotoxic effect. When relative cell count was below 50% of the control condition, no genotoxicity was presented on the graphics to avoid false positive genotoxic results due to apoptosis [19].

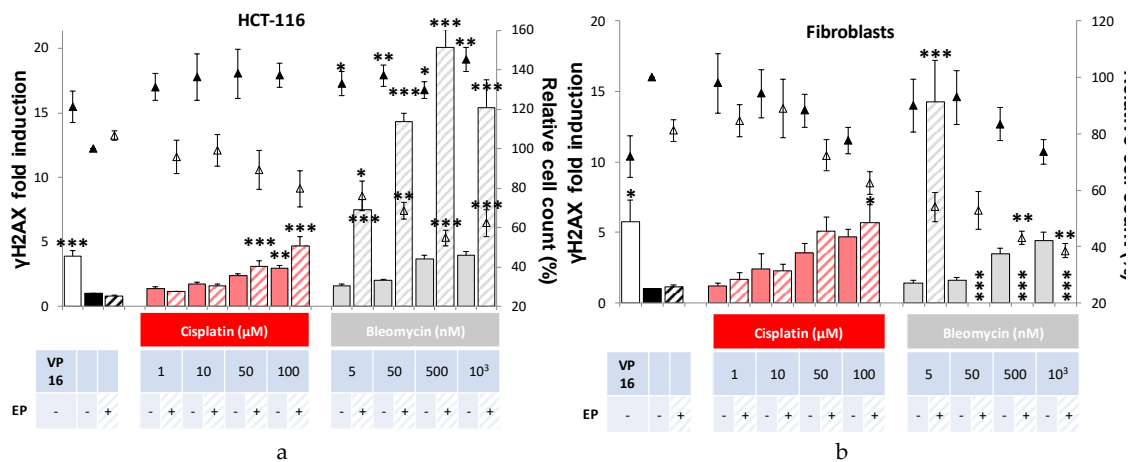


Figure 2. Cytotoxicity and genotoxicity of antitumor drugs bleomycin or cisplatin associated or not with electroporation in HCT-116 tumor cells (a) and normal dermal fibroblasts (b), 24 h after treatment. Cytotoxicity and genotoxicity of increasing concentrations of antitumor drugs cisplatin (red) and bleomycin (gray) associated or not with electroporation (EP). Induction of γ H2AX (histogram) compared with control condition in pulsation buffer. Cytotoxicity associated (hollow triangles) or not (solid triangles) with electroporation is represented by the percentage of relative cell count compared with the control condition (no electroporation). VP16 indicates the positive control (incubation overnight with 3 μ M of etoposide). Experiments were performed at least three times independently, in duplicate. Values represent the mean \pm SEM. Statistically significant increases in H2AX phosphorylation and cytotoxicity after treatment were compared between each condition and its respective control (i.e., drug alone versus control; or drug associated with electric pulses versus EP) using one-way ANOVA followed by Tukey’s post-test. * $p < 0.05$; ** $p < 0.01$, *** $p < 0.001$.

2.3. Calcium Electroporation Induces Cytotoxicity without any Genotoxicity, while Magnesium Electroporation Has No Toxic Effect

Whether in tumor HCT-116 cells or in normal dermal fibroblasts, neither calcium nor magnesium (1, 5, or 10 mM) associated with electroporation induced genotoxicity (Figure 3). When associated with electroporation, 5 and 10 mM calcium induced a statistical significantly reduced cell viability, respectively to 83% and 86% viability in HCT-116, and 13% and 5% viability in dermal fibroblasts. Interestingly, while CaCl₂ and MgCl₂ solutions present the same osmolality, no significant toxic effect of magnesium was observed when associated with electroporation.

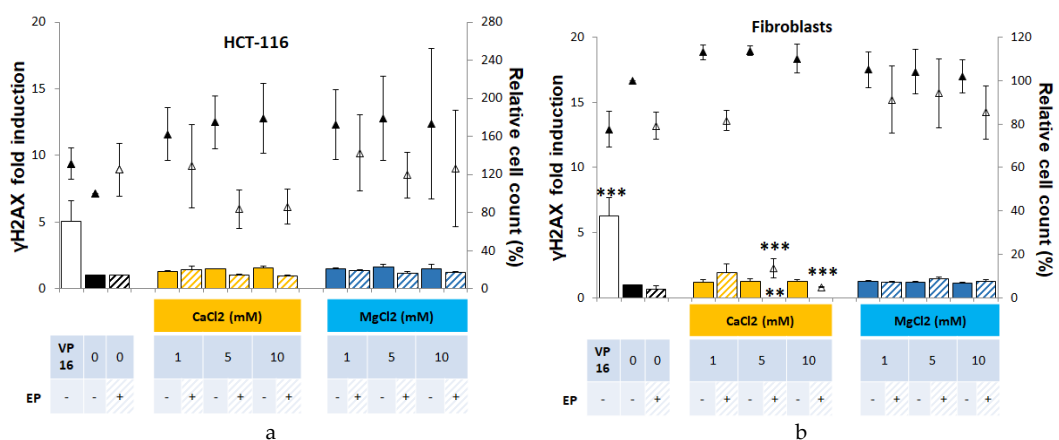


Figure 3. Cytotoxicity and genotoxicity of CaCl₂ or MgCl₂ associated or not with electroporation in HCT-116 (a) and normal dermal fibroblasts (b), 24 h after treatment. Cytotoxicity and genotoxicity of increasing concentrations of CaCl₂ (yellow) and MgCl₂ (blue), associated or not with electroporation

(EP). Induction of γ H2AX (histogram), compared with control condition in HEPES buffer. Cytotoxicity associated (hollow triangles) or not (solid triangles) with electroporation is represented by the percentage of relative cell count compared with the control condition (no electroporation). VP16 indicates the positive control (incubation overnight with 3 μ M etoposide). Experiments were performed at least three times independently, in duplicate. Values represent the mean \pm SEM. Statistically significant increases in H2AX phosphorylation and cytotoxicity after treatment were compared between each condition and its respective control (i.e., drug alone versus control; or drug associated with electric pulses versus EP) using one-way ANOVA followed by Tukey's post-test. * $p < 0.05$; ** $p < 0.01$, *** $p < 0.001$.

2.4. Calcium Electroporation Induces ATP Depletion and Mitochondrial Membrane Depolarization

We analyzed the intracellular ATP content in short time post-treatment (i.e., in 5 min) (Figure 4) as ATP is widely accepted as a reliable and valid marker of cell viability [20]. ATP leakage is associated with plasma membrane electropermeabilization. Therefore, we expected to observe a fall of the intracellular ATP following electroporation alone, but the decrease was not statistically significant 5 min after application of the electric field, indicating an efficient resealing under these electrical conditions; this is in agreement with the fact that under these electrical conditions cells are efficiently permeabilized while their viability remains unaffected (Figure 1). Contrariwise, when electroporation is associated with 5 mM calcium or magnesium, a statistically significant drop in intracellular ATP content was quantified. In HCT-116 cells the decrease of ATP content was around 25% and reached 60% in normal cells.

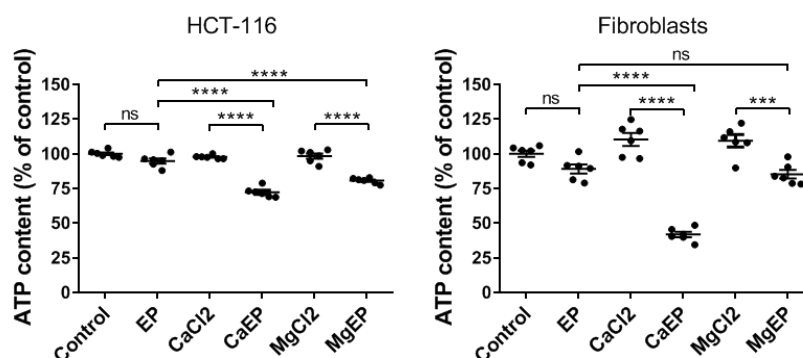


Figure 4. Intracellular ATP depletion within 5 min after electroporation associated with 5 mM calcium. ATP intracellular content was quantified by luminescence assay in HCT-116 cells and dermal fibroblasts. EP: electroporation. Value represents the mean \pm SEM ($n = 6$). Statistical differences were analyzed by one-way ANOVA followed by Tukey's post-test. ns: non-significant. *** $p \leq 0.001$; **** $p \leq 0.0001$.

Observation of mitochondria's ultrastructure indicates that calcium associated to electroporation induced mitochondria swelling and disorganized mitochondrial inner membranes while magnesium associated to electroporation modified the contrast of mitochondria (Figure 5).

We assessed the mitochondrial membrane potential using a fluorescent probe that rapidly accumulates in normal mitochondria (Figure 6). Staining is dependent on mitochondrial membrane potential and is lost when mitochondria become depolarized. A dramatic event leading to mitochondrial membrane depolarization in both normal and tumor cells occurred within 5 min following cell electroporation with calcium, which was not the case with magnesium.

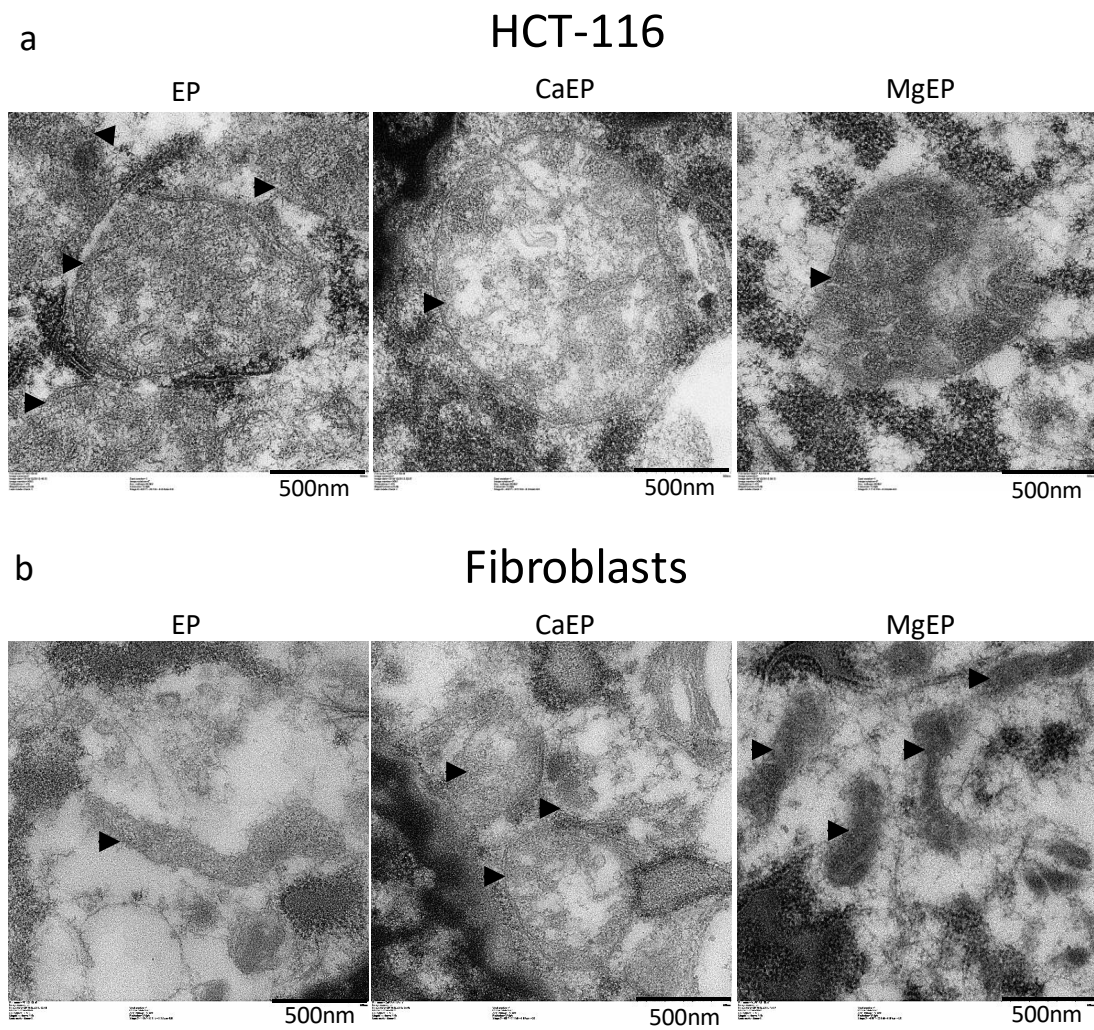


Figure 5. Ultrastructural aspect of mitochondria 5 min post-treatment observed by transmission electron microscopy. (a) HCT-116 tumor cells. (b) Normal dermal fibroblasts. Arrow heads indicate external membrane of mitochondria. Pictures are representative of what was observed in the cell population.

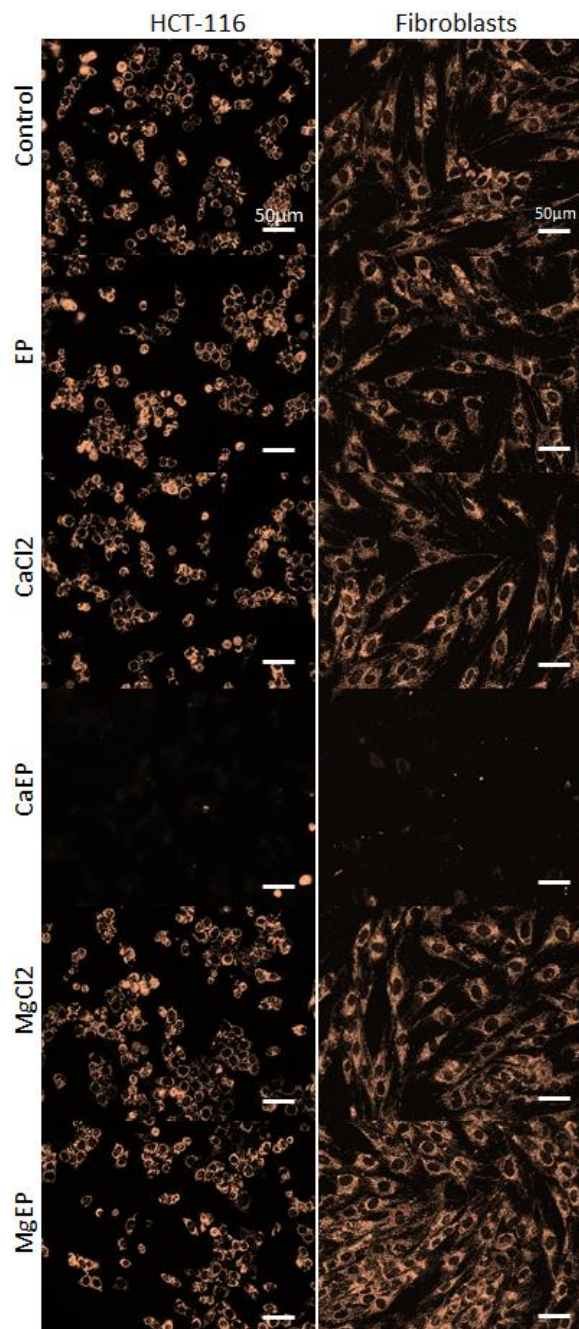


Figure 6. Drastic mitochondrial membrane potential alteration 5 min after electroporation associated with 5 mM calcium. Mitochondrial membrane potential was observed thanks to MitoView633 fluorescent probe in HCT-116 cells and dermal fibroblasts. Representative pictures of two independent experiments.

2.5. Apoptosis Pathway Is Not Induced by Mitochondrial Perturbation Rapidly Observed after Calcium Electroporation

Calcium associated to electroporation displayed a cytotoxic effect as well as a short-term alteration of mitochondria architecture and function that could lead to cell death. For that purpose, apoptosis was assessed in general and more specifically through the mitochondrial pathway (involving caspase-9). Caspase-9, an initiator caspase, is a key player in the mitochondrial pathway of apoptosis initiated in response to agents or insults that trigger, for example, the release of cytochrome c from mitochondria [21]. Caspase-9 and caspases-3/7 activities were quantified over 2 h post treatment with 5 mM CaCl_2 associated

with electroporation (Figure 7). No specific activity of these caspases was observed during this time. Furthermore, despite the rapid and massive alteration of mitochondrial membrane potential within the first minutes following calcium electroporation, no release of cytochrome c was observed after 5 min (Figure 8), which was consistent with the non-activation of caspase-9 over 2 h following the treatment.

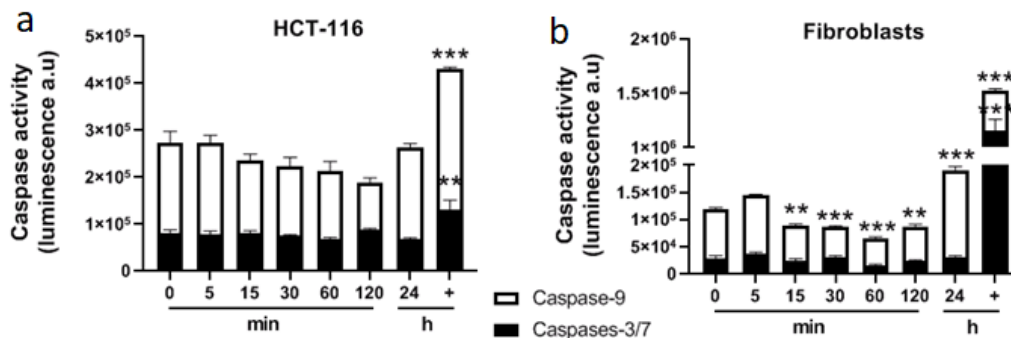


Figure 7. Determination of caspases' activities after 5 mM calcium electroporation in HCT-116 tumor cells (a) and normal dermal fibroblasts (b). Caspase-9 and caspases-3/7 were quantified by luminescence. + indicates the positive control (incubation overnight with staurosporine 1 μ M). Each value represents the mean \pm SEM of at least two independent experiments led in quadruplicate. Statistical differences were analyzed by one-way ANOVA followed by a Dunnett's post-test in comparison to the control condition (0 min). ** $p \leq 0.01$; *** $p \leq 0.0001$.

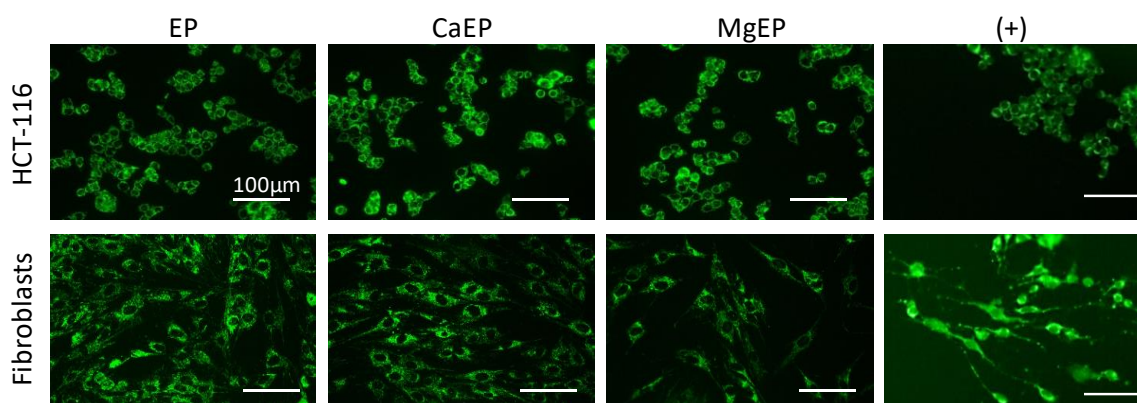


Figure 8. Immunofluorescent detection of cytochrome c 5 min after 5 mM calcium or magnesium electroporation in HCT-116 tumor cells and normal dermal fibroblasts. Punctiform labeling indicates that cytochrome c is sequestered into mitochondria. Indeed, in case of release, the signal is blurry and distributed throughout the cytoplasm, as shown in positive control conditions (+) representing cells incubated for 3 h with 50 μ M staurosporine. Pictures are representative of two independent experiments.

2.6. While Calcium Electroporation Leads to Sustainable Cell Death in Tumor Spheroids, Magnesium Electroporation Solely Temporarily Disaggregates It

We took advantage of the ability of HCT-116 tumor cells to produce homogeneous spheroids to study the response of this 3D tumor tissue model to calcium or magnesium electroporation. Thus, we observed the long-term macroscopic aspect of tumor spheroids to CaCl_2 and MgCl_2 treatments (Video S1). The first observation is that immediately after treatment (the first sequence of the movie) spheroids electroporated with calcium or magnesium swelled and presented blurry margins, contrary to other experimental conditions where spheroids were tightly packed. Spheroids of the control condition without electroporation, 168 mM CaCl_2 and 168 mM MgCl_2 conditions kept growing normally over seven days. The spheroids exposed to electroporation alone presented a macroscopic cohesive aspect but grew slower than the control conditions cited above. After the first culture medium changing (18 h post treatment), a massive detachment of single cells and clusters

of cells from the surface of the spheroids was observed in calcium and magnesium electroporation conditions. Interestingly, two distinct behaviors were observed. The vast majority of detached cells from spheroids treated with calcium electroporation remained inactive. Contrariwise, cellular clusters detached from spheroids treated with magnesium electroporation kept proliferating and moving towards each other to finally fuse together with the original remaining core of the spheroid, forming a giant spheroid. After seven days of experiments, spheroids electroporated with calcium presented a smaller size than all other conditions, contrary to those treated with magnesium associated with electroporation which kept growing. These distinct behaviors are linked to the results obtained on monolayer where calcium electroporation led to high cytotoxicity while magnesium electroporation had no effect on cell viability.

3. Discussion

Even if calcium and magnesium solutions used to treat 2D cells or 3D tumor spheroids presented the same osmolarity, cellular effects at the short-term and long-term were not comparable. These observations underline the major importance of the nature of the ion used to treat cells by electroporation. It was previously reported *in vitro* that at equimolar concentrations, both calcium chloride and calcium glutamate presented the same effects on cytotoxicity when associated with electroporation [22]. Calcium, as a universal carrier of biological information, plays a pivotal role in cell signaling and homeostasis [23]. Electroporation associated to calcium induces a massive influx of this ion within cells, disrupting the intracellular calcium homeostasis. Mitochondrial calcium concentration was shown to regulate respiration, ATP, and reactive oxygen species (ROS) production [24]. These authors demonstrated that micromolar calcium concentrations inhibit the capacity of mitochondria to utilize membrane potential for ATP production. Furthermore, it is known that when intracellular calcium dramatically increases, as is obviously the case after calcium electroporation, Ca²⁺-ATPases rapidly activate and consume the intracellular pool of ATP [25]. This bundle of evidence could explain the massive intracellular ATP depletion observed in our study within minutes after calcium electroporation and that previously reported in the literature on calcium electroporation [8,26,27].

More and more scientific evidences underline the link between ATP production and apoptosis in mitochondria, mediated by its ultrastructure remodeling [28]. In normal conditions, cells are able to maintain stable levels of ATP and mitochondrial membrane potential. However, a long-lasting drop or rise of mitochondrial membrane potential versus normal levels may induce unwanted loss of cell viability [29]. We may assume that the brutal and drastic drop of mitochondrial membrane potential induced by calcium electroporation initiates cellular processes leading to cell death, explaining the high cytotoxic potential of this treatment. In our experimental set-up, we gave evidence that cell death induced by calcium electroporation was not driven by the apoptosis pathway. According to previous studies on calcium electroporation, cellular mechanisms underlying cytotoxic effects of calcium electroporation lay on intracellular ATP depletion and necrosis induction [8,26,27,30].

It has to be underlined that different selectivity to calcium electroporation between normal and cancer cells was observed both in 3D tumor spheroids, *in vivo* and in clinical studies [30–32], while no selectivity of calcium electroporation for cancer cells compared to normal cells was observed in the experimental conditions of our study performed *in vitro* in 2D, where the external volume of calcium is very large compared to the intracellular volume, as already reported in most previous studies [27,33]. All biological observations arising from cell treatment with calcium electroporation (cytotoxicity, ATP intracellular depletion, drop of mitochondrial membrane potential, etc.) were indeed also observed in tumor HCT-116 cells and normal dermal fibroblasts monolayers. Further experiments on distinct tumor cells lines and normal cell types should be led to determine the specificity of calcium electroporation.

Histone H2AX plays a crucial role as a platform on which DNA repair complexes are formed at the sites of DNA damage [34]. Thus, through the *in situ* detection of its phosphorylated form, γ H2AX was proposed as a promising tool in evaluating the genotoxic potential of chemicals [19]. In normal conditions, water-soluble antibiotic bleomycin solely crosses the plasma membrane through

ligand-receptor binding process [35]. However, when associated with electroporation, millions of bleomycin molecules are internalized by cells, leading to a very rapid (within seconds) DNA fragmentation into oligonucleosomal-sized fragments [36]. Depending on the ratio of single strand breaks and double strand breaks induced by bleomycin, cells die by apoptosis, pseudo-apoptosis, or mitotic cell death [37]. In this study, the γ H2AX assay confirmed that cisplatin and bleomycin presented genotoxic and cytotoxic properties, especially when associated with electroporation. It also allowed for quantification of the potentiating effect of electroporation to deliver these drugs. Thus, cisplatin electroporation displayed low advantage contrary to cisplatin alone: one-fold increase of genotoxicity for both HCT-116 and normal dermal fibroblasts whatever the concentration applied. Oppositely, bleomycin electroporation led to 7- and up to 10-fold genotoxicity increase respectively in HCT-116 and fibroblasts compared to bleomycin alone. Thus, electrochemotherapy uses less drugs than conventional chemotherapies to treat cancers with the same efficiency. This difference between compounds may be linked to their physical properties with cisplatin being more effective through diffusion into cells.

In parallel to this observation for known genotoxic agents, this validated method demonstrates for the first time that calcium electroporation displayed an important cytotoxic effect, without generating any genotoxicity. Thanks to these particular characteristics, electroporation associated to calcium could become the gold standard of inexpensive and simple antitumor therapy. Indeed, it is important to keep in mind that with the current anticancer treatments there is more and more remission, but survivors present increased risks of developing secondary malignancies due to the genotoxic effects of the proposed conventional therapies [38]. Thus, a meta-analysis performed on 2,116,163 patients in the USA suffering from the 10 most common cancer sites pointed out that approximately 1 in 12 cancer survivors (8%) develops a second primary malignancy at some point [39].

4. Materials and Methods

4.1. Chemicals

Bleomycin sulfate (Bleo) was purchased from Merck-Millipore (Molsheim, France). PrestoBlue reagent was purchased from Invitrogen Life Technologies (Saint Aubin, France). Cis-diamminedichloroplatinum (II) (Cisplatin, Cispt), calcium chloride (CaCl_2), magnesium chloride (MgCl_2), etoposide (VP16), staurosporine, and propidium iodide (PI) were purchased from Sigma-Aldrich (St Quentin Fallavier, France).

4.2. Cell Culture

Two distinct types of human cells were used. Colorectal tumor cell line HCT-116 was bought from ATCC (#CCL-247) and primary normal dermal fibroblasts were isolated from a 3-year-old foreskin as previously described [40,41]. Both cell types were grown in Dulbecco's modified Eagles medium (Gibco-Invitrogen, Carlsbad, CA, USA) containing Glutamax, 4.5 g/L glucose and pyruvate, supplemented with 10% (v/v) heat inactivated fetal calf serum, 100 U/mL penicillin, and 100 $\mu\text{g}/\text{mL}$ streptomycin. All along the experiments, cells tested negative for mycoplasma (MycoAlert mycoplasma detection kit, Lonza, Walkersville, MD, USA). Cell cultures were maintained in a humidified atmosphere at 37 °C containing 5% CO_2 .

4.3. Tumor Spheroid Production

Three-dimensional (3D) tumor spheroids were produced thanks to the non-adherent technique as previously described [9,42]. Briefly 5000 HCT-116 cells were seeded in ultra-low attachment 96-well plates (Corning, Fisher Scientific, Loughborough, UK). Spheroids were grown for 5 days at 37 °C in a humidified atmosphere containing 5% CO_2 before treatment.

4.4. Electroporation of 2D Monolayers and 3D Tumor Spheroids

Bleomycin and cisplatin drugs were diluted in pulsing buffer (10 mM K_2HPO_4/KH_2PO_4 , 250 mM sucrose, and 1 mM $MgCl_2$ in sterile water, pH 7.4) [14] while, in order to avoid precipitation, $CaCl_2$ and $MgCl_2$ were diluted in HEPES buffer (10 mM HEPES, 250 mM sucrose, and 1 mM $MgCl_2$ in sterile water, pH 7.4) as previously described [8]. For 2D experiments, normal dermal fibroblasts and tumor HCT-116 cells were grown as monolayer in 96-well plates. After washing with phosphate-buffered saline solution (PBS), cells were covered with 50 μ L of pulsing or HEPES buffer containing different concentrations of drugs and incubated for 5 min at room temperature. Two stainless, flat, parallel electrodes (0.35 cm between electrodes) designed specifically to 96-well plate geometry (Megastil, Ljubljana, Slovenia) were applied to the bottom of the well. Defined electric field (8 square-wave pulses of 100 μ s, 1 Hz, and 500 V/cm) was delivered at room temperature by Electro cell S20 generator (LeroyBiotech, Saint Orens de Gameville, France). Special attention was paid to keep constant the time of contact with cytotoxic drugs (bleomycin, cisplatin) or salts ($CaCl_2$ or $MgCl_2$), so that it was the same with and without electroporation (i.e., 6 min). After treatment, cells were washed once with 300 μ L of PBS before addition of 100 μ L of cell culture medium and placed in a humidified atmosphere at 37 °C containing 5% CO_2 until analysis. The concentrations (1, 5, 10 mM) of calcium, and consequently those of magnesium, chosen to treat the cells grown in monolayers were similar to those used in previously published in vitro studies [8,22]. For 3D tumor spheroids experiments, a single spheroid was placed between two stainless steel, flat, parallel electrodes (0.4 cm between electrodes) in 100 μ L of HEPES buffer alone or HEPES buffer containing 168 mM $CaCl_2$ or 168 mM $MgCl_2$. This high calcium concentration was previously chosen for in vivo experiments [8,33] because it corresponds to the concentration of $CaCl_2$ solutions commercially available in hospitals. In addition, when associated to electroporation, 168 mM $CaCl_2$ previously demonstrated efficacy against 3D tumor spheroids in vitro [9]. After 5 min of incubation with $CaCl_2$ or $MgCl_2$ at room temperature, defined electric field allowing transient cell electropermeabilization (8 square-wave pulses of 100 μ s, 1 Hz, and 1000 V/cm) was delivered at room temperature by Electro cell S20 generator as previously described [9]; see Figure A1 for the definition of electric parameters. After treatment, spheroids were washed twice with PBS before being placed in 300 μ L of cell culture medium in a 96-well plate and further placed in a humidified atmosphere at 37 °C containing 5% CO_2 until analysis.

4.5. Determination of Cell Electropermeabilization and Viability after Electroporation

To detect cell electropermeabilization, adherent cells grown in monolayer were submitted to electroporation in pulsation buffer containing 100 μ M propidium iodide which is a non-permeant fluorescent intercalating agent. Once plasma membrane presents defaults, propidium iodide penetrates into the cell, intercalates with DNA, and then exhibits a red fluorescence. Cells were trypsinized immediately after electroporation and PI uptake was quantified by flow cytometry (FACSCalibur, Becton Dickinson, San Jose, CA, USA). Cell viability was assessed 24 h after electroporation alone with PrestoBlue reagent (Invitrogen, Loughborough, UK) according to the manufacturer's instructions. Briefly, 24 h after electroporation, cell culture medium was removed and cells were incubated for 30 min at 37 °C with 100 μ l of 1 \times PrestoBlue reagent diluted in PBS, before reading absorbance on a plate reader at 570 nm and 600 nm (CLARIOstar, BMG Labtech, Ortenberg, Germany). For every set of experiments, three biological replicates were produced and analyzed.

4.6. Osmolarity Measurement

The osmolarity of calcium and magnesium solutions was measured using a cryoscopic osmometer, OSMOMAT 030 (Gonotec, Berlin, Germany) according to the manufacturer's protocol. Four distinct solutions of 5 mM $CaCl_2$ or $MgCl_2$ in HEPES buffer used along all the experiments were measured. Osmolarity of calcium and magnesium solutions used to treat cells were measured with a cryoscopic

osmometer. Solutions of HEPES buffer with 5 mM CaCl₂ or MgCl₂ presented an osmolarity of respectively 326.3 ± 31.5 and 341.8 ± 12.8 mOsmol/L, which was statistically similar (unpaired t-test, $p = 0.3973$).

4.7. Genotoxicity and Cytotoxicity

Genotoxicity and cytotoxicity were determined thanks to the published γ H2AX In-Cell Western technique and performed as previously described [19,43,44]. Briefly, HCT-116 tumor cells and normal dermal fibroblasts were seeded 24 h prior to treatment at a respective density of 30,000 and 15,000 cells per well in a 96-well plate. A positive control was added to the plate and consisted of cells incubated for 24 h with 3 μ M etoposide (VP16), a known genotoxic drug. Controls conditions were respectively pulsing buffer alone for bleomycin and cisplatin conditions and HEPES buffer for CaCl₂ and MgCl₂ conditions. As described above, special attention was paid to the time of contact with the drug (bleomycin, cisplatin, CaCl₂, or MgCl₂), so that it was the same with and without electroporation. Then 24 h after treatment, cells were fixed with 4% paraformaldehyde (Electron Microscopy Science) in PBS and chemically permeabilized with 0.2% Triton X-100. Cells were then incubated in blocking solution (MAXblock Blocking Medium supplemented phosphatase inhibitor PHOSSTOP and 0.1 g/L RNase A) prior to 2 h incubation at room temperature with rabbit monoclonal anti- γ H2AX primary antibody (Clone 20E3, Cell Signaling). Detection was carried out with an infrared fluorescent dye conjugated to goat antibody (CF770, Biotium, Hayward, CA, USA). For DNA labeling, RedDot2 (Biotium) was added simultaneously to the secondary antibody. After 1 h of incubation at room temperature, the fluorescence was read using an Odyssey Infrared Imaging Scanner (Li-CorScienceTec, Les Ulis, France). The fluorescence corresponding to γ H2AX and co-localizing with RedDot2 was integrated in the constant area corresponding to the one located in-between the electrodes during application of the electric field and expressed as fold change compared with controls in pulsing or HEPES buffer. Cell viability was calculated by relative cell count (final cell count (treated)/final cell count (control) × 100) assessed by automated fluorescence. Genotoxicity was considered positive when the tested treatment produced a statistically significant 1.6-fold γ H2AX induction at a level of cytotoxicity above 50% compared to the control. These parameters were based on previous studies based on the use of γ H2AX quantification [19,44–48]. All experiments were performed at least three times independently, in duplicate. Error bars represent the mean ± SEM. Statistically significant increases in H2AX phosphorylation and cytotoxicity after treatment were compared between the same drug concentration, associated or not with electroporation using one-way ANOVA followed by Tukey's post-test (* $p < 0.05$; ** $p < 0.01$).

4.8. ATP Quantification

Intracellular ATP content was quantified 5 min after calcium or magnesium electroporation thanks to CellTiter-Glo Luminescent Cell Viability Assay (Promega, Madison, WI, USA) according to the manufacturer's protocol. This assay uses ATP as a co-factor for luciferase reaction. In brief, 15,000 dermal fibroblasts or 30,000 tumor HCT-116 cells grown in monolayers in 96-well plates for 24 h were incubated 5 min in HEPES buffer containing 5 mM of CaCl₂ or MgCl₂, then exposed to electroporation, incubated for 5 min at room temperature, and then washed once with PBS. First, 25 μ L of cell culture medium were added and immediately after, 25 μ L of reagent were added. The plate was shaken for 2 min on an orbital shaker and then incubated 10 min in the dark at room temperature. Then 40 μ L of supernatant were transferred in a white 96-well plate before reading on a luminescence plate reader (CLARIOstar, BMG Labtech, Ortenberg, Germany). Statistical differences between each condition containing six biological replicates were analyzed by one-way ANOVA followed by Tukey's post-test.

4.9. Transmission Electron Microscopy

For an ultrastructural examination of organelles, cells were grown in monolayer on round glass coverslips. Since cells are not supposed to grow on glass, these coverslips were coated with gelatin (Fisher Scientific) chosen because of its high biocompatibility with cells [49]. Then 5 min after calcium or

magnesium electroporation, coverslips were plunged in 2% glutaraldehyde in 0.1 M Sorensen phosphate buffer (pH 7.4) and then further processed for transmission electron microscopy. Finally, pictures of ultra-thin sections stained with uranyl acetate were acquired on a Hitachi HT7700 microscope (Hitachi High-Technologies Corp., Tokyo, Japan).

4.10. Mitochondrial Membrane Potential

Mitochondrial membrane potential was assessed using MitoView 633 (Biotium) which is a mitochondrial membrane potential-sensitive, fluorogenic dye that rapidly accumulates in mitochondria. Staining is dependent on mitochondrial membrane potential and lost when mitochondria become depolarized. Cells were labeled according to the manufacturer's protocol. Briefly, cells grown in monolayer were washed with PBS and then incubated for 20 min in the dark in a humidified atmosphere at 37 °C containing 5% CO₂ with 50 nM MitoView 633 in cell culture medium. Cells were then washed twice in PBS and submitted to calcium electroporation as described above. Then 5 min after treatment, fluorescence pictures (excitation 622 nm/emission 648 nm) of tumor and normal cells were acquired with a wide-field fluorescence DMIRB Leica microscope coupled to a Photometrics Cool SNAP HQ camera.

4.11. Quantification of Caspases 9 and 3/7 Activities

Caspases 9 and 3/7 activities were quantified respectively with Caspase-Glo 9 assay and Caspase-Glo 3/7 assay according to the manufacturers' protocol (Promega). These assays are based on luminogenic substrates of caspases 9 or 3/7 and the signal generated is proportional to the amount of caspase activity present. Briefly, 15,000 dermal fibroblasts or 30,000 tumor HCT-116 cells grown in monolayers in 96-well plates for 24 h were incubated 5 min in HEPES buffer containing 5 mM of CaCl₂, then exposed to electroporation, washed twice in PBS, covered with 50 µL of cell culture medium, and then placed in a humidified atmosphere at 37 °C containing 5% CO₂ for the chosen time. After 0, 5, 15, 30, 60, 120 min or 24 h, 50 µL of reagent were added directly into the wells, incubated for 30 min at room temperature and then 90 µL of supernatant were transferred in a white 96-well plate before reading on a luminescence plate reader (CLARIOstar, BMG Labtech). A positive control (cells incubated overnight with 1 µM staurosporine) was added to the experiment to check the quality of the test and cell susceptibility to apoptosis.

4.12. Immunofluorescent Detection of Cytochrome c

In order to visualize if cytochrome c was released from mitochondria after calcium electroporation treatment, 15,000 dermal fibroblasts or 30,000 tumor HCT-116 cells were grown in monolayers in 96-well plates for 24 h. They were then incubated for 5 min in HEPES buffer containing 5 mM of CaCl₂ or MgCl₂, and exposed to electroporation. Then 5 min after electroporation treatment, cells were washed twice in PBS, and fixed 1 h at room temperature with paraformaldehyde 4%. Cytochrome c was then immunodetected using mouse monoclonal antibody against cytochrome c (Cell Signaling #12963, clone 6H2.B4, dilution 1/300). A positive control for mitochondrial apoptosis leading to cytochrome c release was added (cells incubated 3 h with 50 µM staurosporine).

Three-dimensional (3D) tumor spheroids growth and integrity after 168 mM CaCl₂ and MgCl₂ electroporation. Videos presenting the macroscopic aspect of spheroids until 7 days post treatment were obtained on a JuliStage video microscope (NanoEnTek, Waltham, MA, USA). Pictures were taken every 1 h over 7 days. Cell culture media changed at 18 h and 139 h.

5. Conclusions

Calcium associated to electroporation allows supra-physiological doses of calcium to enter the cytosol and induces mitochondrial dysfunction leading to cell death. Contrary to what is observed with classical antitumor drugs, such as cisplatin and bleomycin, calcium electroporation does not induce genotoxicity in exposed cells, and therefore turns out to be an inexpensive, efficient, simple, and safe innovative cancer treatment.

Supplementary Materials: The following are available online at <http://www.mdpi.com/2072-6694/12/2/425/s1>, Video S1: Long-term macroscopic aspect of tumor spheroids to CaCl_2 and MgCl_2 associated to electroporation treatments.

Author Contributions: Conceptualization, M.A. and M.-P.R.; methodology, L.G., M.A., and M.-P.R.; validation, L.G., M.A., and M.-P.R.; formal analysis, L.G.; investigation, L.G., I.F., A.M., and H.B.; writing—original draft preparation, L.G.; writing—review and editing, L.G., M.A., and M.-P.R.; visualization, L.G. and I.F.; supervision, M.A. and M.-P.R.; project administration, M.-P.R.; funding acquisition, L.G. and M.-P.R. All authors have read and agreed to the published version of the manuscript.

Funding: This research was funded by SILAB-Jean Paufigue foundation (LG) and NUMEP Plan Cancer PC201615 grant (MPR).

Acknowledgments: The authors acknowledge the “Toulouse Réseau Imagerie” core IPBS facility support (Genotoul, Toulouse, France), and CMEAB (TRI-Genotoul platform) is gratefully acknowledged for TEM experiments. We also would like to thank Géraldine Alberola and Muriel Golzio for scientific discussions. Research was conducted in the scope of the EBAM European Associated Laboratory (LEA) and resulted from the networking efforts of the COST Action TD1104.

Conflicts of Interest: The authors declare no conflicts of interest. The funding body did not play any role in the design of the study and collection, analyses, and interpretation of data and in writing the manuscript.

Appendix A

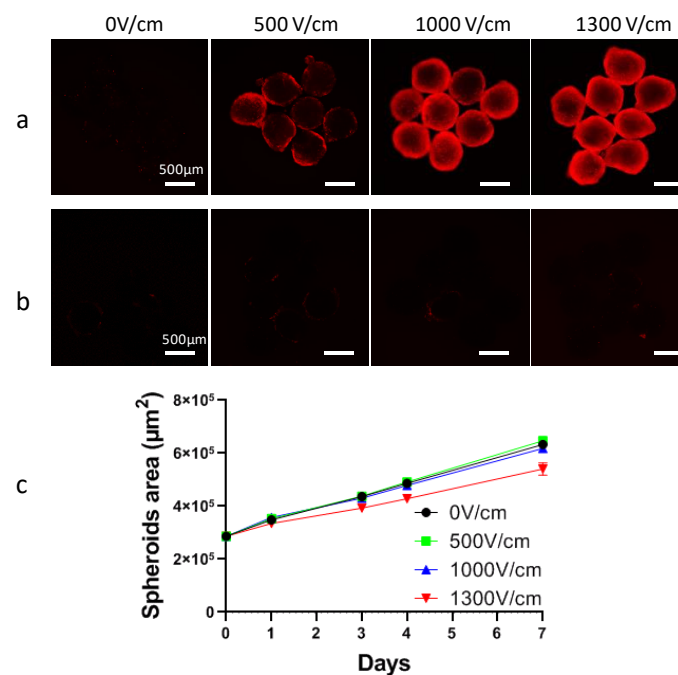


Figure A1. Determination of optimal voltage for HCT-116 spheroid's electroporation. (a) Cell electroporation within the spheroid was globally assessed by propidium iodide (PI) penetration. For that purpose, at least 6 spheroids were submitted to an external electric field (8 pulses lasting 100 µs at 1 Hz frequency) with increasing intensity in pulsation buffer supplemented with 100 µM PI. PI fluorescence was recorded immediately after electroporation using an AxioObserver wide field fluorescence microscope (Zeiss, Marly-le-roi, France). (b) Plasma membrane resealing, ensuring that electroporation was reversible, was tested by incubating at least 6 spheroids with 100 µM PI 30 min after electroporation application. (c) Tumor spheroid growth curves were recorded over 7 days after application of electroporation with increasing electric field strength. Fixed number (×8), frequency (1 Hz), and duration (100 µs) of pulses were used; solely electric field intensity was modified in this experiment. Further, 1000 V/cm and 1300 V/cm conditions, respectively used in [9] and [14] induced an efficient cell electroporation, which was not the case for 500 V/cm condition (a). None of these three voltages induced irreversible electroporation since no permeabilized cells were observed 30 min after electroporation (b). Finally, the following growth of the spheroid indicated that 1300 V/cm significantly alter spheroids' growth, explaining why we chose 1000 V/cm condition.

References

1. Yarmush, M.L.; Golberg, A.; Serša, G.; Kotnik, T.; Miklavčič, D. Electroporation-Based Technologies for Medicine: Principles, Applications, and Challenges. *Annu. Rev. Biomed. Eng.* **2014**, *16*, 295–320. [[CrossRef](#)] [[PubMed](#)]
2. Gehl, J.; Sersa, G.; Matthiessen, L.W.; Muir, T.; Soden, D.; Occhini, A.; Quaglino, P.; Curatolo, P.; Campana, L.G.; Kunte, C.; et al. Updated standard operating procedures for electrochemotherapy of cutaneous tumours and skin metastases. *Acta Oncol.* **2018**, *57*, 874–882. [[CrossRef](#)] [[PubMed](#)]
3. Neumann, E.; Rosenheck, K. Permeability changes induced by electric impulses in vesicular membranes. *J. Membr. Biol.* **1972**, *10*, 279–290. [[CrossRef](#)] [[PubMed](#)]
4. Orłowski, S.; Belehradec, J.; Paoletti, C.; Mir, L.M. Transient electropermeabilization of cells in culture: Increase of the cytotoxicity of anticancer drugs. *Biochem. Pharmacol.* **1988**, *37*, 4727–4733. [[CrossRef](#)]
5. Miklavčič, D.; Mali, B.; Kos, B.; Heller, R.; Serša, G. Electrochemotherapy: From the drawing board into medical practice. *Biomed. Eng. Online* **2014**, *13*, 29. [[CrossRef](#)] [[PubMed](#)]
6. Rebersek, M.; Cufar, T.; Cemazar, M.; Kranjc, S.; Sersa, G. Electrochemotherapy with cisplatin of cutaneous tumor lesions in breast cancer. *Anticancer. Drugs* **2004**, *15*, 593–597. [[CrossRef](#)] [[PubMed](#)]
7. Jafari, S.M.S.; Lak, F.J.; Gazdhar, A.; Shafiqhi, M.; Borradori, L.; Hunger, R.E. Application of electrochemotherapy in the management of primary and metastatic cutaneous malignant tumours: A systematic review and meta-analysis. *Eur. J. Dermatol.* **2018**, *28*, 287–313.
8. Frandsen, S.K.; Gissel, H.; Hojman, P.; Tramm, T.; Eriksen, J.; Gehl, J. Direct Therapeutic Applications of Calcium Electroporation to Effectively Induce Tumor Necrosis. *Cancer Res.* **2012**, *72*, 1336. [[CrossRef](#)]
9. Frandsen, S.K.; Gibot, L.; Madi, M.; Gehl, J.; Rols, M.-P. Calcium Electroporation: Evidence for Differential Effects in Normal and Malignant Cell Lines, Evaluated in a 3D Spheroid Model. *PLoS ONE* **2015**, *10*, e0144028. [[CrossRef](#)]
10. Falk, H.; Forde, P.F.; Bay, M.L.; Mangalanathan, U.M.; Hojman, P.; Soden, D.M.; Gehl, J. Calcium electroporation induces tumor eradication, long-lasting immunity and cytokine responses in the CT26 colon cancer mouse model. *Oncoimmunology* **2017**, *6*. [[CrossRef](#)]
11. Falk, H.; Matthiessen, L.W.; Wooler, G.; Gehl, J. Calcium electroporation for treatment of cutaneous metastases; a randomized double-blinded phase II study, comparing the effect of calcium electroporation with electrochemotherapy. *Acta Oncol. Stockh. Swed.* **2018**, *57*, 311–319. [[CrossRef](#)] [[PubMed](#)]
12. Plaschke, C.C.; Gehl, J.; Johannesen, H.H.; Fischer, B.M.; Kjaer, A.; Lomholt, A.F.; Wessel, I. Calcium electroporation for recurrent head and neck cancer: A clinical phase I study. *Laryngoscope Investig. Otolaryngol.* **2019**, *4*, 49–56. [[CrossRef](#)] [[PubMed](#)]
13. Marrero, B.; Heller, R. The use of an in vitro 3D melanoma model to predict in vivo plasmid transfection using electroporation. *Biomaterials* **2012**, *33*, 3036–3046. [[CrossRef](#)] [[PubMed](#)]
14. Gibot, L.; Wasungu, L.; Teissié, J.; Rols, M.-P. Antitumor drug delivery in multicellular spheroids by electropermeabilization. *J. Control. Release* **2013**, *167*, 138–147. [[CrossRef](#)] [[PubMed](#)]
15. Znidar, K.; Bosnjak, M.; Jesenko, T.; Heller, L.C.; Cemazar, M. Upregulation of DNA Sensors in B16.F10 Melanoma Spheroid Cells after Electrotransfer of pDNA. *Technol. Cancer Res. Treat.* **2018**, *17*. [[CrossRef](#)] [[PubMed](#)]
16. Pampaloni, F.; Reynaud, E.G.; Stelzer, E.H.K. The third dimension bridges the gap between cell culture and live tissue. *Nat. Rev. Mol. Cell Biol.* **2007**, *8*, 839. [[CrossRef](#)]
17. Marty, M.; Sersa, G.; Garbay, J.R.; Gehl, J.; Collins, C.G.; Snoj, M.; Billard, V.; Geertsen, P.F.; Larkin, J.O.; Miklavcic, D.; et al. Electrochemotherapy – An easy, highly effective and safe treatment of cutaneous and subcutaneous metastases: Results of ESOPE (European Standard Operating Procedures of Electrochemotherapy) study. *Eur. J. Cancer Suppl.* **2006**, *4*, 3–13. [[CrossRef](#)]
18. Kopp, B.; Khoury, L.; Audebert, M. Validation of the γ H2AX biomarker for genotoxicity assessment: A review. *Arch. Toxicol.* **2019**, *93*, 2103–2114. [[CrossRef](#)]
19. Khoury, L.; Zalko, D.; Audebert, M. Validation of high-throughput genotoxicity assay screening using γ H2AX in-cell western assay on HepG2 cells. *Environ. Mol. Mutagen.* **2013**, *54*, 737–746. [[CrossRef](#)]
20. Riss, T.L.; Moravec, R.A.; Niles, A.L.; Duellman, S.; Benink, H.A.; Worzella, T.J.; Minor, L. Cell Viability Assays. In *Assay Guidance Manual*; Sittampalam, G.S., Coussens, N.P., Brimacombe, K., Grossman, A., Arkin, M., Auld, D., Austin, C., Baell, J., Bejcek, B., Caaveiro, J.M.M., et al., Eds.; Eli Lilly & Company; The National Center for Advancing Translational Sciences: Bethesda, MD, USA, 2004.

21. Li, P.; Zhou, L.; Zhao, T.; Liu, X.; Zhang, P.; Liu, Y.; Zheng, X.; Li, Q. Caspase-9: Structure, mechanisms and clinical application. *Oncotarget* **2017**, *8*, 23996–24008. [[CrossRef](#)]
22. Frandsen, S.K.; Gissel, H.; Hojman, P.; Eriksen, J.; Gehl, J. Calcium electroporation in three cell lines: A comparison of bleomycin and calcium, calcium compounds, and pulsing conditions. *Biochim. Biophys. Acta BBA Gen. Subj.* **2014**, *1840*, 1204–1208. [[CrossRef](#)]
23. Brini, M.; Cali, T.; Ottolini, D.; Carafoli, E. Intracellular calcium homeostasis and signaling. *Met. Ions Life Sci.* **2013**, *12*, 119–168.
24. Fink, B.D.; Bai, F.; Yu, L.; Sivitz, W.I. Regulation of ATP production: Dependence on calcium concentration and respiratory state. *Am. J. Physiol. Cell Physiol.* **2017**, *313*, C146–C153. [[CrossRef](#)]
25. Berridge, M.J.; Bootman, M.D.; Roderick, H.L. Calcium signalling: Dynamics, homeostasis and remodelling. *Nat. Rev. Mol. Cell Biol.* **2003**, *4*, 517. [[CrossRef](#)]
26. Hansen, E.L.; Sozer, E.B.; Romeo, S.; Frandsen, S.K.; Vernier, P.T.; Gehl, J. Dose-dependent ATP depletion and cancer cell death following calcium electroporation, relative effect of calcium concentration and electric field strength. *PLoS ONE* **2015**, *10*, e0128034. [[CrossRef](#)]
27. Staresinic, B.; Jesenko, T.; Kamensek, U.; Krog Frandsen, S.; Sersa, G.; Gehl, J.; Cemazar, M. Effect of calcium electroporation on tumour vasculature. *Sci. Rep.* **2018**, *8*, 9412. [[CrossRef](#)]
28. Burke, P.J. Mitochondria, Bioenergetics and Apoptosis in Cancer. *Trends Cancer* **2017**, *3*, 857–870. [[CrossRef](#)]
29. Zorova, L.D.; Popkov, V.A.; Plotnikov, E.Y.; Silachev, D.N.; Pevzner, I.B.; Jankauskas, S.S.; Babenko, V.A.; Zorov, S.D.; Balakireva, A.V.; Juhaszova, M.; et al. Mitochondrial membrane potential. *Mitochondrial Biochem. Bioenerget.* **2018**, *552*, 50–59. [[CrossRef](#)]
30. Frandsen, S.K.; Krüger, M.B.; Mangalanathan, U.M.; Tramm, T.; Mahmood, F.; Novak, I.; Gehl, J. Normal and Malignant Cells Exhibit Differential Responses to Calcium Electroporation. *Cancer Res.* **2017**, *77*, 4389–4401. [[CrossRef](#)]
31. Frandsen, S.K.; Gehl, J. A Review on Differences in Effects on Normal and Malignant Cells and Tissues to Electroporation-Based Therapies: A Focus on Calcium Electroporation. *Technol. Cancer Res. Treat.* **2018**, *17*. [[CrossRef](#)]
32. Szewczyk, A.; Gehl, J.; Daczewska, M.; Saczko, J.; Frandsen, S.K.; Kulbacka, J. Calcium electroporation for treatment of sarcoma in preclinical studies. *Oncotarget* **2018**, *9*, 11604–11618. [[CrossRef](#)]
33. Frandsen, S.K.; Gehl, J. Effect of calcium electroporation in combination with metformin in vivo and correlation between viability and intracellular ATP level after calcium electroporation in vitro. *PLoS ONE* **2017**, *12*, e0181839. [[CrossRef](#)]
34. Bonner, W.M.; Redon, C.E.; Dickey, J.S.; Nakamura, A.J.; Sedelnikova, O.A.; Solier, S.; Pommier, Y. GammaH2AX and cancer. *Nat. Rev. Cancer* **2008**, *8*, 957–967. [[CrossRef](#)]
35. Pron, G.; Belehradek, J.; Mir, L.M. Identification of a Plasma Membrane Protein That Specifically Binds Bleomycin. *Biochem. Biophys. Res. Commun.* **1993**, *194*, 333–337. [[CrossRef](#)]
36. Tounekti, O.; Pron, G.; Belehradek, J.; Mir, L.M. Bleomycin, an Apoptosis-mimetic Drug That Induces Two Types of Cell Death Depending on the Number of Molecules Internalized. *Cancer Res.* **1993**, *53*, 5462.
37. Tounekti, O.; Kenani, A.; Foray, N.; Orłowski, S.; Mir, L.M. The ratio of single- to double-strand DNA breaks and their absolute values determine cell death pathway. *Br. J. Cancer* **2001**, *84*, 1272–1279. [[CrossRef](#)]
38. Simard, J.L.; Kircher, S.M.; Didwania, A.; Goel, M.S. Screening for Recurrence and Secondary Cancers. *Care Cancer Surviv.* **2017**, *101*, 1167–1180. [[CrossRef](#)]
39. Donin, N.; Filson, C.; Drakaki, A.; Tan, H.-J.; Castillo, A.; Kwan, L.; Litwin, M.; Chamie, K. Risk of second primary malignancies among cancer survivors in the United States, 1992 through 2008. *Cancer* **2016**, *122*, 3075–3086. [[CrossRef](#)]
40. Gibot, L.; Galbraith, T.; Kloos, B.; Das, S.; Lacroix, D.A.; Auger, F.A.; Skobe, M. Cell-based approach for 3D reconstruction of lymphatic capillaries in vitro reveals distinct functions of HGF and VEGF-C in lymphangiogenesis. *Biomaterials* **2016**, *78*, 129–139. [[CrossRef](#)]
41. Gibot, L.; Galbraith, T.; Huot, J.; Auger, F.A. A Preexisting Microvascular Network Benefits In vivo Revascularization of a Microvascularized Tissue-Engineered Skin Substitute. *Tissue Eng. Part A* **2010**, *16*, 3199–3206. [[CrossRef](#)]
42. Gibot, L.; Rols, M.-P. 3D spheroids' sensitivity to electric field pulses depends on their size. *J. Membr. Biol.* **2013**, *246*, 745–750. [[CrossRef](#)]

43. Theumer, M.G.; Henneb, Y.; Khoury, L.; Snini, S.P.; Tadriss, S.; Canlet, C.; Puel, O.; Oswald, I.P.; Audebert, M. Genotoxicity of aflatoxins and their precursors in human cells. *Toxicol. Lett.* **2018**, *287*, 100–107. [[CrossRef](#)] [[PubMed](#)]
44. Quesnot, N.; Rondel, K.; Audebert, M.; Martinais, S.; Glaise, D.; Morel, F.; Loyer, P.; Robin, M.-A. Evaluation of genotoxicity using automated detection of γ H2AX in metabolically competent HepaRG cells. *Mutagenesis* **2016**, *31*, 43–50. [[CrossRef](#)] [[PubMed](#)]
45. Khoury, L.; Zalko, D.; Audebert, M. Complementarity of phosphorylated histones H2AX and H3 quantification in different cell lines for genotoxicity screening. *Arch. Toxicol.* **2016**, *90*, 1983–1995. [[CrossRef](#)] [[PubMed](#)]
46. Ando, M.; Yoshikawa, K.; Iwase, Y.; Ishiura, S. Usefulness of Monitoring γ -H2AX and Cell Cycle Arrest in HepG2 Cells for Estimating Genotoxicity Using a High-Content Analysis System. *J. Biomol. Screen.* **2014**, *19*, 1246–1254. [[CrossRef](#)]
47. Bryce, S.M.; Bemis, J.C.; Mereness, J.A.; Spellman, R.A.; Moss, J.; Dickinson, D.; Schuler, M.J.; Dertinger, S.D. Interpreting in vitro micronucleus positive results: Simple biomarker matrix discriminates clastogens, aneugens, and misleading positive agents: Interpreting In vitro Micronucleus Positive Results. *Environ. Mol. Mutagen.* **2014**, *55*, 542–555. [[CrossRef](#)]
48. Smart, D.J.; Ahmedi, K.P.; Harvey, J.S.; Lynch, A.M. Genotoxicity screening via the γ H2AX by flow assay. *Mutat. Res. Mol. Mech. Mutagen.* **2011**, *715*, 25–31. [[CrossRef](#)]
49. Figarol, A.; Gibot, L.; Golzio, M.; Lonetti, B.; Mingotaud, A.-F.; Rols, M.-P. A journey from the endothelium to the tumor tissue: Distinct behavior between PEO-PCL micelles and polymersomes nanocarriers. *Drug Deliv.* **2018**, *25*, 1766–1778. [[CrossRef](#)]



© 2020 by the authors. Licensee MDPI, Basel, Switzerland. This article is an open access article distributed under the terms and conditions of the Creative Commons Attribution (CC BY) license (<http://creativecommons.org/licenses/by/4.0/>).